Kihara, T., Takashi, E., Yamamura, K., & Tabushi, I. (1982) *Biochim. Biophys. Acta 702*, 249–253.
Kitagawa, T., Nagai, K., & Tsubaki, M. (1979) *FEBS Lett. 104*, 376–378.
Lecomte, J. T. J., & La Mar, G. N. (1985) *Biochemistry 24*, 7388–7395.
Morikis, D. (1990) Ph.D. Thesis, Northeastern University, Boston, MA.
Morikis, D., Champion, P. M., Springer, B. A., & Sligar, S. G. (1989) *Biochemistry 28*, 4791–4800.
Moffat, K., Deatherage, J. R., & Seyberg, D. W. (1979) *Science 206*, 1035–1042.
Murray, L., Hofrichter, J., Henry, E., & Eaton, W. (1988) *Biophys. Chem. 29*, 63–76.
Nagai, K., Luisi, B., Shih, D., Miyazaki, G., Imai, K., Poyart, C., De Young, A., Kwiatkowski, L., Noble, R. W., Lin, S.-H., & Yu, N.-T. (1987) *Nature 329*, 858.
Olson, J. S., Mathews, A. J., Rohlfs, R. J., Springer, B. A., Egeberg, K. D., Sligar, S. G., Tame, J., Renaud, J.-P., & Nagai, K. (1989) *Nature 336*, 265–266.
Puett, D. (1973) *J. Biol. Chem. 248*, 4623–4634.
Sage, J. T., Morikis, D., & Champion, P. M. (1991) *Biochemistry* (preceding paper in this issue).
Shen, L. L., & Hermans, J., Jr. (1972) *Biochemistry 11*, 1836–1849.
Smulevich, G., Miller, M. A., Gosztola, D., & Spiro, T. G. (1989) *Biochemistry 28*, 9905–9908.
Šrajer, V., Reinisch, L., & Champion, P. M. (1988) *J. Am. Chem. Soc. 110*, 6656–6670.
Traylor, T. G., Dearduff, L. A., Coletta, M., Ascenzi, P., Antonini, E., & Brunori, M. (1983) *J. Biol. Chem. 258*, 12147–12148.
White, D. K., Cannon, J. B., & Traylor, T. G. (1979) *J. Am. Chem. Soc. 101*, 2443–2454.

Two-Dimensional NMR and Structure Determination of Salmon Calcitonin in Methanol†

Robert P. Meadows,‡ Edward P. Nikonowicz,‡ Claude R. Jones,‡ James W. Bastian,§ and David G. Gorenstein*,‡

Department of Chemistry, Purdue University, West Lafayette, Indiana 47907, and 126 Chestnut Street, Park Forest, Illinois 60466

Received August 9, 1990; Revised Manuscript Received October 25, 1990

ABSTRACT: The structure of the 32-residue peptide salmon calcitonin (sCT) in 90% MeOH–10% H_2O has been investigated by two-dimensional NMR techniques and molecular modeling. Sequential assignments for nearly all of the 32 spin systems have been obtained, and results indicate that the heptaresidue loop formed by the disulfide bond between Cys-1 and Cys-7 is followed by an α-helical segment from Val-8 through Tyr-22. A region of conformational heterogeneity is observed for residues 20–25, resulting from the slow isomerism of the cis and trans forms of Pro-23. The C-terminal segment is found to exist in an extended conformation.

Salmon calcitonin I (sCT) is a 32 amino acid peptide which is physiologically important for inhibiting activity of osteoclasts (Niall et al., 1969; Kallio et al., 1972). It is administered by daily injection for the treatment of osteoporosis (Wallach et al., 1977), Pagets disease (Avramides et al., 1974), hypercalcemia (Hosking & Weller, 1986), and reflex sympathetic dystrophy (Gobelet, 1986). Known forms of calcitonin include those produced by the parafollicular cells of the thyroid (human, rat, pig, sheep, and cow) and those from the ultimobranchial glands of salmon (I, II, and III), eel, and chicken (Potts et al., 1972; Azria, 1989). Ultimobranchial calcitonins, tested in mammals, are approximately 30-fold more potent than calcitonins of thyroidal origin, yet all are 32 amino acids in length having an amino-terminal 1–7 disulfide bridge and a carboxyl-terminal proline amide (Azria, 1989). The primary sequence of sCT is shown in Figure 1.

Information on the conformation of calcitonin in the presence of its receptor should permit design of analogues having fewer side effects and better absorbability when given by noninjectable routes. Epand et al., using circular dichroism, have shown the amphiphilic sCT to have little secondary structure in water but to exhibit significant α-helix in the presence of dimyristoylphosphatidylglycerol (DMPG) or 90% MeOH/10% water (Epand et al., 1983; Orlowski et al., 1987). NMR investigations of other membrane-active peptides, in particular the studies of δ-hemolysin, have shown that there may be little difference in structures produced in methanolic solvents and those resulting from the more complicated lipid micellar environments (Inagaki et al., 1989). Thus, our initial investigations into the conformation of sCT were performed in 90% MeOH in the expectation that the results may have relevance to that of the conformation of calcitonin in the presence of its lipid-bound receptor.

Materials and Methods

Calcitonin was prepared by solid-phase chemistry, was purified by preparative HPLC, and was the generous gift of Armour Pharmaceutical, Kankakee, IL. NMR samples were prepared by dissolving the lyophilized sCT peptide in ~650

† Supported by the NIH (A127744), the Purdue University Biochemical Magnetic Resonance Laboratory which is supported by the National AIDS Research Center at Purdue (AI7277713), and the NSF Biological Facilities Center on Biomolecular NMR, Structure and Design at Purdue (BBS 8614177 and DIR-9000360).

‡ Purdue University.
§ Park Forest, IL.

0006-2960/91/0430-1247$02.50/0

Cys[1]-Ser-Asn-Leu-Ser[5]-Thr-Cys[7]-Val-Leu-Gly[10]-Lys-

-Leu-Ser-Gln-Glu[15]-Leu-His-Lys-Leu-Gln[20]-Thr-Tyr-

-Pro-Arg-Thr[25]-Asn-Thr-Gly-Ser-Gly[30]-Thr-Pro-NH_2

FIGURE 1: Primary amino acid sequence of salmon calcitonin I (sCT).

μL of either 90% CD_3OD/10% D_2O or 90% CD_3OH/10% H_2O to a concentration of 6 mM. The solutions were buffered with 30 mM CD_3COOD and adjusted to an uncorrected pH meter reading of pH 3.1 with a glass electrode. CD_3OH was prepared by distillation from 100% CD_3OD and 0.1 M HCl.

^{1}H NMR spectra were recorded on a Varian VXR500S or Varian VXR600S spectrometer operating at ambient temperature at 500 and 600 MHz, respectively. Spectra were processed with VNMR and were internally referenced to the residual HDO peak at 4.76 ppm. For the 10% H_2O samples, the water peak was suppressed with a CW preirradiation pulse during the relaxation delay period.

Phase-sensitive COSY (Jeener et al., 1979) spectra were collected with 4096 t_2 data points and 512 real t_1 increments with the States method of phase cycling. A total of 16 scans per FID were collected with a recovery delay of 2.5 s. Phase-sensitive DQF-COSY (Piantini et al., 1982; Muller et al., 1986) spectra were collected similarly to the COSY except that 32 transients per FID were acquired. Apodization typically consisted of a combination of sine-bell and Gaussian functions. The triple quantum filtered COSY (TQF-COSY) was collected at 600 MHz with 4096 t_2 points (96 transients) and 512 real t_1 increments, zero filled to 2096 points in t_1, and apodized in both dimensions with a small Gaussian function. Coupling constants were determined from the peak to peak separation of the multiplets in the DQF-COSY spectrum.

TOCSY spectra (Braunschweiler & Ernst, 1983; Davis & Bax, 1985) were obtained with 4096 data points in the t_2 dimension and 512 real t_1 increments at mixing times of 30, 100, and 200 ms. As above, the data were treated with a combination of sine-bell and Gaussian apodization in both dimensions prior to Fourier transformation. No sample heating was detected during the MLEV-17 spin-lock periods.

NOESY spectra (Kumar et al., 1981) were collected with 4096 data points in the t_2 dimension and 512 real t_1 increments with the States method of phase cycling. A total of 32 transients per FID were collected with a relaxation delay time of 4 s. Mixing times of 80, 200, 400, and 500 ms were collected. All spectra were zero filled to 2048 in the t_1 dimension prior to Fourier transformation and apodized with a shifted sine-bell function for assignment purposes or simple line broadening for integration of NOESY volumes.

An aliquot of the protonated methanolic NMR sample was taken and diluted to a concentration of 0.13 mM with buffer, and the CD spectrum was acquired on a JASCO 600 CD/ORD spectrometer. An ellipticity of $[\theta]_{222} = -12\,100$ was recorded.

Generation of the initial structure for molecular dynamics was done with the model-building/refinement program SYBYL (Tripos Association Inc). Energy minimizations and molecular dynamics were carried out with the molecular mechanics/dynamics program AMBER (Weiner & Kollman, 1981). Gas-phase dynamics at 300 K were performed with a constraining force constant of 40 kcal mol^{-1} Å^{-2} in a flat-well modification of the AMBER potential (Gorenstein et al., 1990). The dynamics simulations were allowed to continue for 40 ps with coordinates obtained every 50 fs. A distance-dependent dielectric potential was employed. Special residues included in the simulation were the protonated carboxyl group of Glu-16 and the C-terminal amidated Pro-32. Visualization and plot generation of the model structures was performed with the molecular modeling program MIDAS (Ferrin & Langridge, 1980) operating on a Silicon Graphics 4D Personal Iris computer.

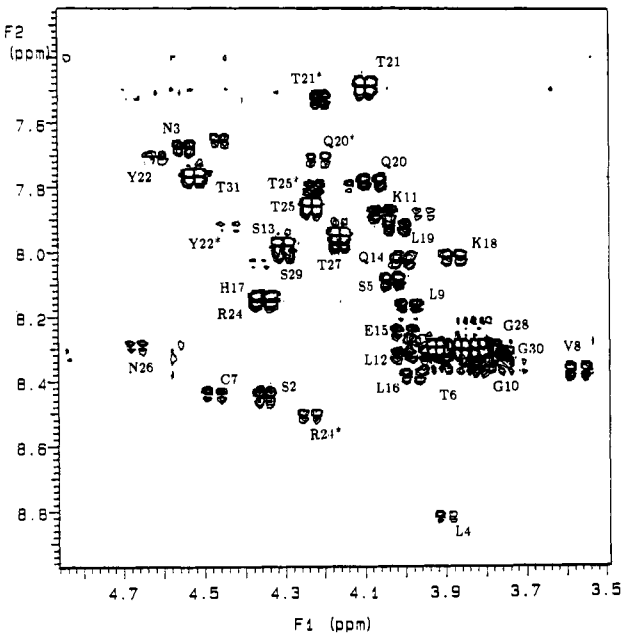

FIGURE 2: Fingerprint region of the DQF-COSY for sCT in MeOH. Resonances noted with an asterisk (*) are assigned to the "alternate" conformation.

RESULTS

Assignment of the proton signals of sCT was accomplished with the sequential assignment methodology outlined by Wuthrich (1986). Spin systems, protons within a residue coupled through a scalar network, were identified from the COSY and TOCSY spectra. Connectivities between spin systems were obtained by identifying NOEs (through-space interactions) between protons of adjacent residues. Finally, structural information was gathered on the basis of the patterns of connectivities between sequential and nonsequential residues once the assignments had been determined.

Spin System Identification. The assignment procedure involves the identification of individual spin system types, categorization of the spin systems into amino acid types, and finally assignment of the spin system to a specific amino acid in the primary sequence. Identification of these spin systems is begun by locating those systems having unique coupling or chemical shift properties. Several amino acids give rise to unique spin systems and/or chemical shift patterns. For instance, unique scalar connectivity is exhibited by Gly, the only amino acid having a pair of resonances that are three-bond scalar coupled to the peptide NH. Characteristic chemical shift information may be exhibited by serine residues which have a pair of Hβ resonances in the 3.3–4.3 ppm range, while cystine has Hβs typically found between 2.5 and 3.6 ppm (Grob & Kalbitzer, 1988). Thus, in our effort to elucidate the sequential assignment of sCT, we first looked for unique spin systems, then opened the search to include simple spin systems such as the AMX patterns of Cys, Asn, Tyr, and His, and finally located the long side-chain systems of Leu, Lys, Glu, Gln, and Pro.

To begin, we attempted to locate the Ser, Thr, and Gly residues, a total of 12 spin systems. Shown in Figure 2 is the NH–Hα or fingerprint region of the COSY spectrum (for

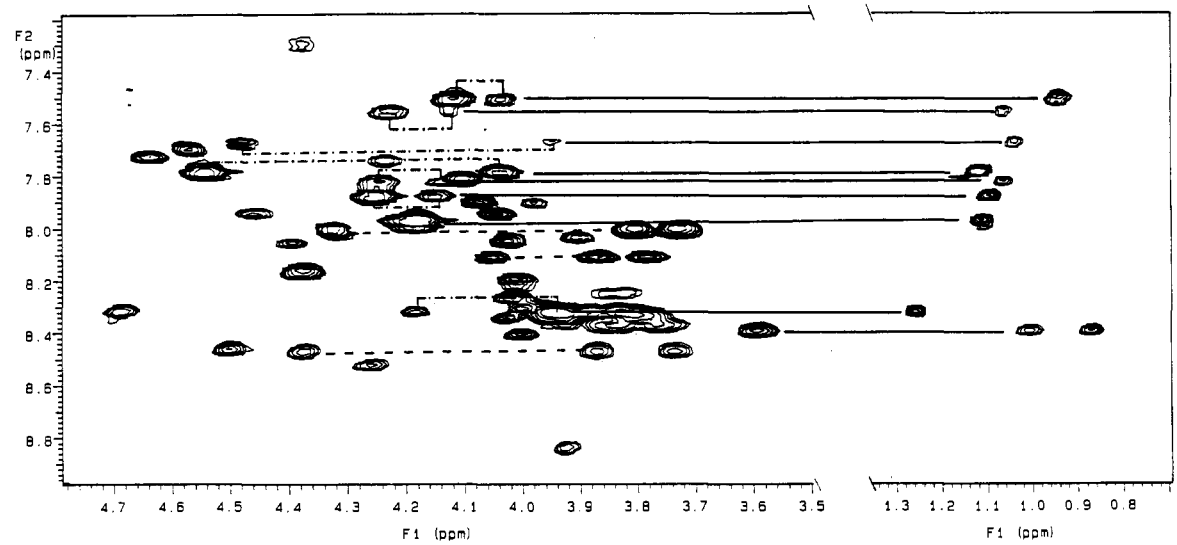

FIGURE 3: Fingerprint and NH–CH_3 region of the 100-ms TOCSY spectrum for sCT in MeOH. Dashed lines connect serine Hα and Hβs; dotted-dashed lines connect the threonone Hα to Hβ; solid lines connect threonine CH_3 to Hα and Hβ and Val-8 CH_3 (pair) to Val-8 Hα.

comparison, Figure 3 shows a similar region of the 100-ms TOCSY spectrum). The serine resonances are clearly assignable from the additional pairs of peaks in the fingerprint region of the TOCSY spectrum which arise from the four-bond scalar coupling of NH–Hβ and NH–Hβ'. Unfortunately, two serines are completely coincident in chemical shift. Coincident serine resonances were also reported for sCT in DMSO (Motta et al., 1989).

Threonine spin systems exhibit characteristic cross peaks in the fingerprint region of the TOCSY spectrum resulting from the NH–Hβ four-bond correlation and a strong NH–CH_3 connectivity (see Figure 3). However, the presence of eight threonine spin systems was noted whereas the primary sequence contains only five threonine residues. COSY spectra in the Hα–CH_3 region show seven well-resolved threonine spin systems. Because the HPLC trace suggests that the NMR sample was pure (data not shown), the additional spin systems result from conformational heterogeneity (see also Figure 5). Conformational heterogeneity for sCT has been observed in DMSO and has been ascribed to the relatively slow isomerization of the cis and trans forms of Pro 23 (Motta et al., 1989). It is perhaps not unexpected to observe a similar phenomenon in MeOH.

The three Gly residues were unassignable at this point due to chemical shift overlap. It was thought that the peptide NHs were buried within the crowded region at $\approx$8.30 ppm. This was verified in the triple quantum filtered COSY (Figure 4). These resonances were assigned at a later stage (see Sequential Assignments).

Two separate AMX patterns for tyrosine were observed although the primary sequence contains only a single tyrosine residue, further supporting the notion of conformational heterogeneity. Interestingly, the ^{1}H one-dimensional spectrum gives clear indication of the conformational states of the sCT in MeOH. Observed in Figure 5 are expansions of the one-dimensional spectra for sCT in MeOD and MeOH. Clearly visible in the spectrum obtained in fully deuterated solvent are the resonances for the *o,m*-protons of a tyrosine in an alternate conformation. Integration of the peak areas gives a value of $\sim$30% for the second conformation.

The single valine resonance was easily located in the TOCSY and COSY spectra, as was Arg, an $A_2(T_2)$MPX spin system (Wuthrich, 1986). The Cys, Asn, and His spin systems were identified in the usual manner as were Leu, Lys, and Pro.

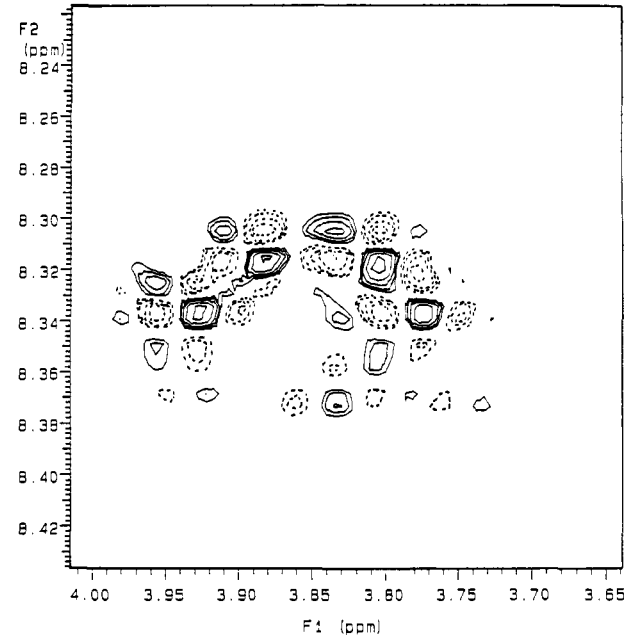

FIGURE 4: Expansion of the fingerprint region of the triple quantum filtered COSY.

However, we note the presence of four spin systems indicative of Glx residues whereas the primary sequence contains only two Gln and one Glu residue.

Sequential Assignments. Sequential assignments were made from NOESY spectra acquired at 80 and 200 ms. Since the single valine residue was identified unambiguously in the spin system analysis, it is an obvious starting point for the sequential assignment. From Val-8 it should be possible to trace the sequential connectivity back through the cyclic heptapeptide region to the N-terminus and then forward through the remainder of the primary sequence.

The sequential connectivity trace for Cys-1 to Leu-9 is given in the fingerprint region of the 200-ms NOESY (Figure 6). Interestingly, the Hβ proton of Thr-6 appears downfield of its Hα. This was verified in the DQF-COSY and is not anomalous (Grob & Kalbitzer, 1988).

Although the cross peak connecting Leu-9 and Gly-10 is not observable in the fingerprint region, one may "backtrack" to the Gly-10 Hα and Hα' via the NOEs between the NH of

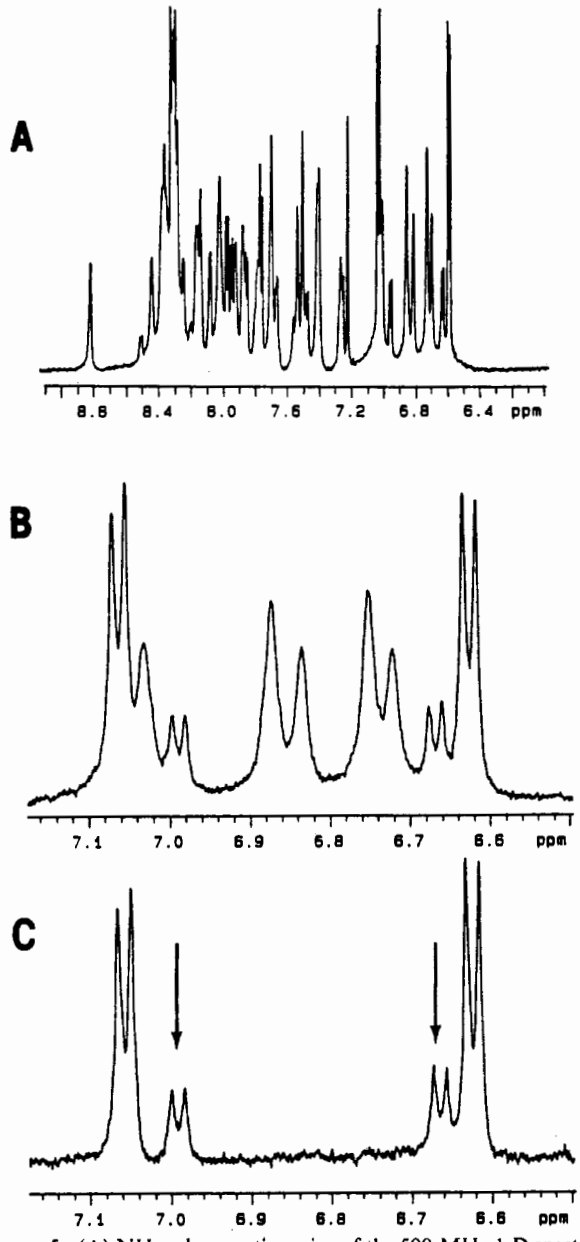

FIGURE 5: (A) NH and aromatic region of the 500-MHz 1-D spectrum of sCT in MeOH. (B) Expansion of aromatic region in MeOH. (C) Same region as in (B) but in fully deuterated MeOD. Clearly evident are the (o,m) resonances for Tyr-22 and the alternate conformation Try-22* (arrows).

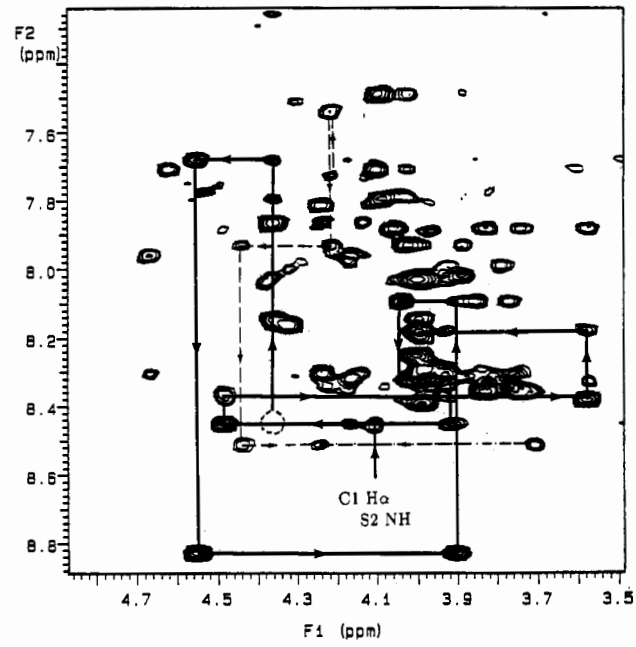

FIGURE 6: Fingerprint region of the 500-MHz NOESY spectrum (200 ms) for sCT in MeOH. Solid line traces Cys-1 to Leu-9 (dotted circle represents the position of Ser-2 NH–Hα COSY cross peak). Dashed lines connect residues Gln-20* (alternate conformation) to Thr-25*. Dotted-dashed line is NOESY connectivity for Pro-23* Hδ to Arg-24* NH.

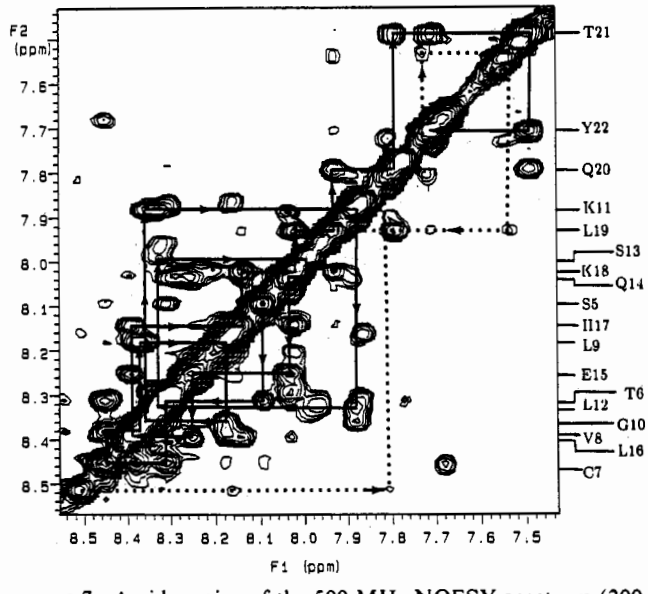

FIGURE 7: Amide region of the 500-MHz NOESY spectrum (200 ms) for sCT in MeOH. Sequential traces are shown for residues 5–22 (solid lines) and residues 20*–25* (dotted lines). Residue 5 is denoted with an asterisk.

Lys-11 and a pair of protons at 3.78 and 3.58 ppm. These chemical shifts are coincident with the Hα and Hα′ of one of the glycines identified in the TQF-COSY and serve to assign Gly-10. Since the fingerprint region is considerably overlapped, it is not surprising that the Leu-9 Hα to Gly-10 NH cross peak is not distinct. Additionally, two weak NOEs are observed from side-chain protons of Leu-9 to NH of Gly-10. Close inspection of the NH–NH region revealed the presence of a medium-intensity connectivity from Leu-9 to Gly-10 and from Gly-10 to Lys-11. The assignment of Leu-12 is confirmed by a sequential NOE between the Hβ and Hγ of Lys-11 and the NH of a leucine spin system (Leu-12). Further connectivity is observed as a strong NOE between these two spin systems in the NH–NH region. At this point, because of chemical shift degeneracy, the sequential assignment is lost.

The connectivity is picked up again at Gln-14. The ambiguity of the Glx spin system assignment is removed when one looks at the cross peaks for the side-chain protons of Gln-14 to Glu-15. Several medium-intensity cross peaks from the NH of a Glx residue to the side-chain protons of another Glx spin system are observed. These are the adjacent Glx pair Gln-14 and Glu-15. Further, one of the Glx spin systems has side-chain NOEs to the NH of an unassigned leucine spin system. From the direction of the pattern, it is concluded that the amide protons at 8.02, 8.26, and 8.40 ppm are those for Gln-14, Glu-15, and Leu-16, respectively. Further verification comes in the NH–NH region with medium-intensity sequential connectivities (Figure 7). The connectivity pattern for residues 16–23 was straightforward, and a sequential assignment trace for residues 5–22 in the NH–NH region is given in Figure 7.

Proline-23 was easily identified from an NOE between Tyr-22 NH and the Hδ resonance of a proline spin system.

Table I: ^{1}H NMR Assignments of sCT in 90% CD_3OH

	^{1}H chemical shifts (ppm)			
residue	NH	Hα	Hβ	others
Cys[1]		4.08	3.48, 3.02	
Ser[2]	8.46	4.39	3.87, 3.71	
Asn[3]	7.67	4.55	3.02, 2.93	γNH$_2$ 7.04, 7.72
Leu[4]	8.83	3.91	1.54, 1.54	γCH 1.52; δCH$_3$ 0.83, 0.81
Ser[5]	8.12	4.03	3.86, 3.75	
Thr[6]	8.31	3.89	4.15	γCH$_3$ 1.25
Cys[7]	8.46	4.49	3.09, 3.09	
Val[8]	8.38	3.58	2.12	γCH$_3$ 1.00, 0.85
Leu[9]	8.18	4.00	1.72, 1.70	γCH 1.50; δCH$_3$ 0.80, 0.80
Gly[10]	8.37	3.78, 3.58		
Lys[11]	8.03	4.04	1.92, 1.92	γCH 1.44, 1.44; δ 1.62, 1.62; ε 2.84, 2.84
Leu[12]	8.33	4.02	1.70, 1.70	γCH 1.61; δCH$_3$ 0.81, 0.81
Ser[13]	8.05	4.34	3.81, 3.72	
Gln[14]	8.04	4.01	2.10, 2.10	γ 2.50, 2.27; δNH$_2$
Glu[15]	8.25	4.01	2.19, 2.04	γ 2.39, 2.37
Leu[16]	8.40	4.02	1.45, 1.45	γCH 1.71; δCH$_3$ 0.78, 0.78
His[17]	8.15	4.39	3.25, 3.25	4H 7.24; 2H 8.30
Lys[18]	8.04	3.90	1.92, 1.92	γCH 1.34, 1.34; δ 1.56, 1.56; ε 2.78, 2.78
Leu[19]	7.95	4.04	1.80, 1.80	γCH 1.53; δCH$_3$ 0.85, 0.81
Gln[20]	7.81	4.08	2.14, 2.02	γ 2.48, 2.28; εNH$_2$ 7.42, 6.74
Gln[20]*	7.73	4.14	2.06, 2.06	γ 2.44, 2.30; εNH$_2$ 7.42, 6.71
Thr[21]	7.49	4.08	4.01	γCH$_3$ 0.88
Thr[21]*	7.54	4.20	4.10	γCH$_3$ 1.09
Tyr[22]	7.73	4.60	2.95, 2.93	*o* 6.62; *m* 7.06
Tyr[22]*	7.92	4.45	2.92, 2.86	*o* 6.67; *m* 6.96
Pro[23]		4.32	2.14, 1.93	γ 1.85, 1.85, ε 3.74, 3.62
Arg[24]	8.16	4.38	1.86, 1.69	γ 1.56, 1.54; δ 3.25, 3.13, ε 7.28
Arg[24]*	8.51	4.24	1.80, 1.80	γ 1.52, 1.52; δ 3.15, 3.15
Thr[25]	7.87	4.24	4.04	γCH$_3$ 1.09
Thr[25]*	7.83	4.22	4.04	γCH$_3$ 1.12
Asn[26]	8.31	4.68	2.76, 2.68	γNH$_2$ 7.51, 6.85
Thr[27]	7.96	4.14	4.12	γCH$_3$ 1.12
Gly[28]	8.34	3.94, 3.79		
Ser[29]	7.96	4.34	3.81, 3.72	
Gly[30]	8.31	3.90, 3.82		
Thr[31]	7.97	4.52	4.04	γCH$_3$ 1.04
Pro[32]				

Arginine 24 was established unambiguously in the spin system identification, and Thr-25 through Ser-29 were sequentially assigned. Interestingly though, two weak-intensity NOEs from the Hα of Pro-23 are observed; one each to the peptide NH and side-chain amide protons of Asn-26.

The remaining threonine (Thr-31) is assigned from the observance of a weak NOE from an Hα of an unassigned glycine, Gly-30, and the connectivity is corroborated with a weak-intensity in the NH–NH region connecting the two resonances. The C-terminal proline is unidentified. Table I summarizes the chemical shifts of sCT in MeOH.

Sequential Assignments for the Alternate Conformation. From the 1-D and fingerprint region of the COSY spectra it is noted that a portion of sCT maintains a region of conformational heterogeneity. The sequential pathway for several of the residues in the second conformation can be followed in the usual manner. Spin systems in an alternate conformation may be identified and assigned from residues 20–25. Figure 6 illustrates the assignment trace for residues in this second conformation (see also Figure 7). Note that, in cases where chemical shift degeneracy is observed (for instance, Gln-20*-Thr-21* Hαs), the sequential assignment was verified in other spectral regions, particularly the NH–NH region of the 200-ms NOESY.

It is noted that the final unassigned (and weakest intensity) Glx spin system has a medium NH–NH NOE to an unassigned threonine spin system, putatively Thr-21* (where the asterisk denotes the alternate conformation species). Additionally, an Hα(*i*) to NH(*i*+1) cross peak may be observed between these two spin systems. A medium Hα(*i*) to NH(*i*+1) NOE from Thr-21 to the unassigned, low-intensity tyrosine resonance identifies Tyr-22*. An NH–NH connectivity confirms the assignment. Also, an (*i*,*i*+2) NOE in the amide region connects Gln-20* and Tyr-22*. A medium-intensity (*i*,*i*+2) NH–Hα NOE connects Tyr-22* to an unidentified and weak-intensity Arg spin system, thus assigning Arg-24*. The peptide NH of Arg-24* is seen to have a medium-intensity NOE from the Hδ of a proline spin system, perhaps Pro-23*. Finally, a weak NH–NH connectivity is observed between Arg-24* and an unassigned threonine spin system, giving us Thr-25*. Interestingly, medium-intensity cross peaks are observed for Gln-20*–Tyr-22* and Gln-20*–Thr-25* in the NH–NH region of the 200-ms NOESY. Finally, the re-

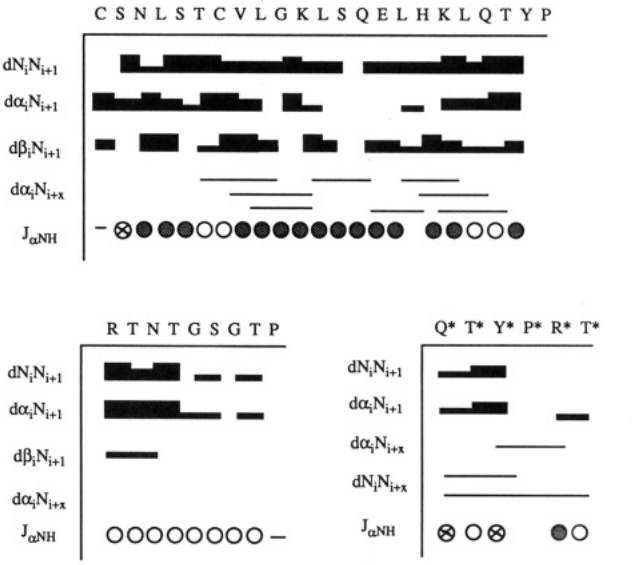

FIGURE 8: Summary of the NOEs and coupling constant data for sCT in MeOH. The one-letter code for the residue is given at the top. Relative size of the NOEs is defined by the size of the bar. Long-range NOEs are given as connecting lines (*i*,*i*+*x*, where *x* > 2). Coupling constant data are given for the peak to peak separation in the 500-MHz DQF-COSY. Measured values are <6.5 Hz (●), 6.5 < *J* < 9.0 Hz (○), and >9.0 Hz (⊗). Residues marked with an asterisk show alternate conformation species.

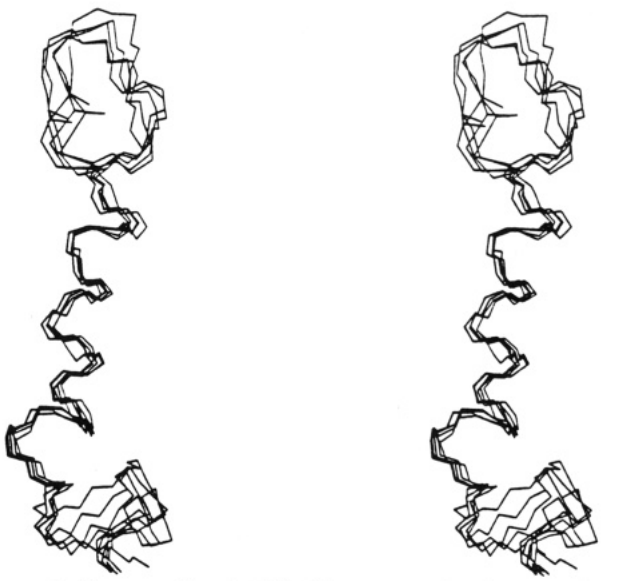

FIGURE 9: Stereo overlay of sCT backbone atoms taken from snapshots at 32, 34, 36, 38, and 40 ps of the NOESY distance-restrained molecular dynamic simulations starting from a model containing an α-helical segment from residue 8 to residue 22.

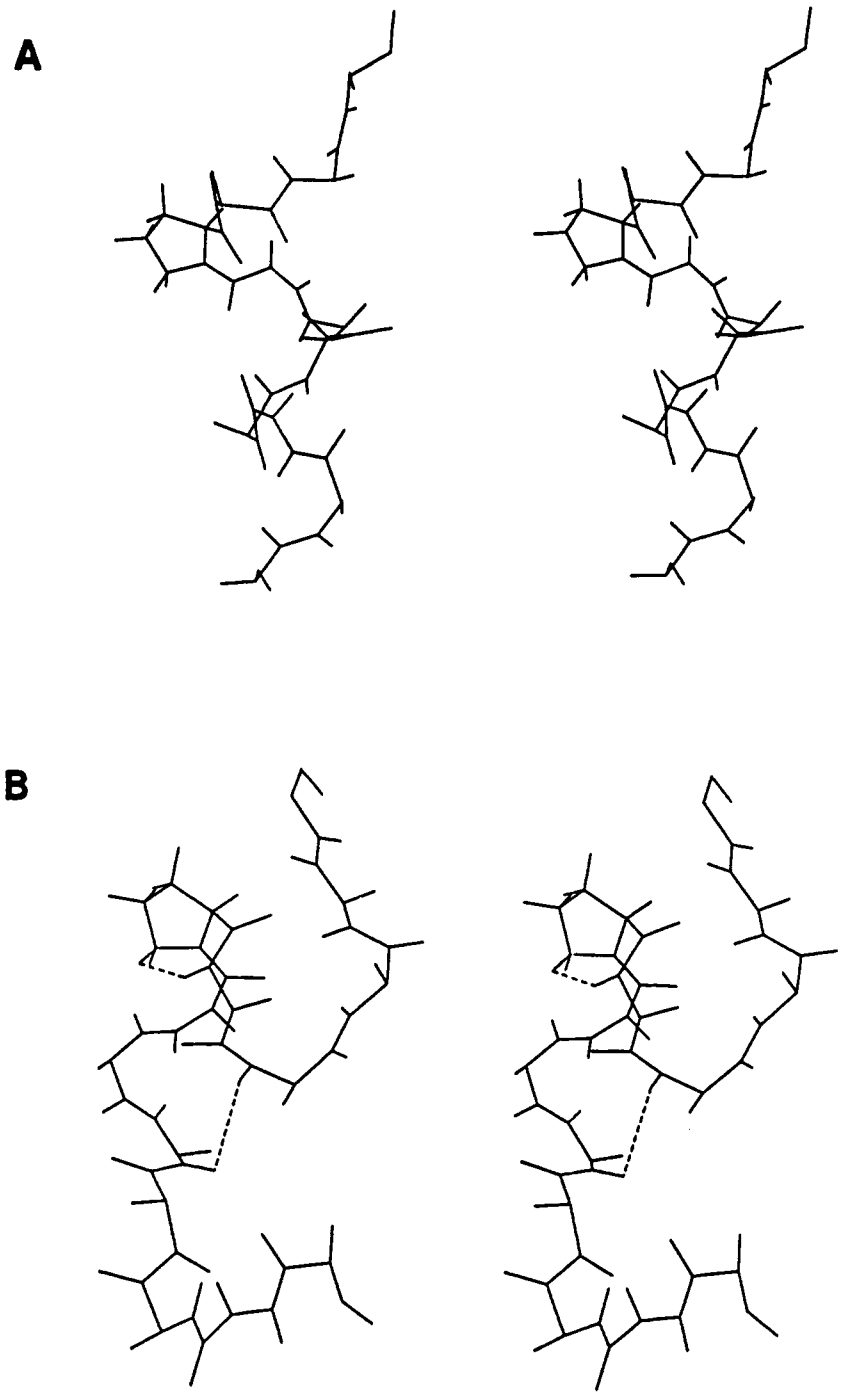

FIGURE 10: Backbone heavy atoms and protons for residues 16–26 of sCT taken from snapshots at 38 ps of molecular dynamics for the (A) major conformation structure helical model and (B) the minor conformation helical model. Dashed lines in the minor conformer show 25 NH–20 NH (2.00 Å) and 24 NH–23 HD2 (2.90 Å).

maining unassigned Thr cross peak may be assigned to Thr-31*, which may arise from cis/trans isomerization about Pro-32.

Importantly, the N–H of Tyr-22 has a weak NOE to the Hδ proton of Pro-23 while Tyr-22* does not. Further, while Arg-24 does not exhibit any NOEs to Pro-23, Arg-24* has a medium–strong NOE to Pro-23* Hδ. These NOE intensity differences are entirely consistent with our assignment of the main conformer to the *trans*-Pro-23 peptide and the minor conformer (*) to the *cis*-Pro-23 peptide.

Discussion

Observations concerning the secondary structure of peptides and proteins can be made on the basis of the qualitative information contained in the interresidue NOESY cross-peak network. Medium–weak-intensity NOE peaks of the forms $d_{\alpha N}(i,i+4)$,$d_{\alpha N}(i,i+3)$,$d_{NN}(i,i+2)$, and $d_{NN}(i,i+1)$ are generally indicative of α-helical structure (the latter two also would be found in tight turns), while strong NOE cross peaks of the form $d_{\alpha N}(i,i+1)$ are indicative of β-sheet-type structure (Wuthrich, 1986).

The heptapeptide loop region of sCT shows a large number of interresidue NOEs of medium to strong intensity. Interestingly, some of these NOEs are from residues within the disulfide to residues further along in the primary sequence; both Thr-6 and Cys-7 show long-range NOE (T6–L9 and C7–K11). Thus, one may speculate that the residues in the C-terminal end of the disulfide loop are acting as a template

upon which higher-order secondary structures may develop. Support for this notion comes from the observation that several of the residues in the loop region have been shown to act in an N-capping capacity, that is, to stabilize the N-terminus of an α-helix (Richardson & Richardson, 1990). Indeed, threonine, serine, and asparagine (perhaps Thr-6, Ser-5, Ser-2, and Asn-3) have been shown to have good ability in stabilizing the N-terminus of an α-helix.

α-Helical character is strongly evident from residues 8–22. Medium-intensity NOE for NH–NH (Figure 7) and (Hα–NH(i,i+2 and i,i+3) and coupling constants (for the most part) on the order of 6 Hz or less indicate an ordered secondary structure throughout all or part of the sequence from residue 8 to residue 22. The H_α–NH(i,i+1) cross-peak intensities in β-sheet structures are strong, and since the observed NOEs of sCT in MeOH are typically medium or even weak in intensity at 80 and 200 ms, it is unlikely that sCT forms a β-sheet in 90% methanol. Evidence for helicity is also obtained from the circular dichroism $[\theta]_{222}$ value measured for our NMR sample (−12 100). While this is a smaller rotation than those reported for sCT in MeOH (Orlowski et al., 1987; $[\theta]_{222}$ = −16 000), it is certainly indicative of α-helix. A summary of the NOE and coupling constant data is presented in Figure 8.

A model geometry was generated on the basis of the NMR observations. The model thus contained an α-helical segment as described above for residues 8–22 and random conformation for all other residues. This model geometry was subjected to 40 ps of constrained molecular dynamics with pseudoenergy constraints derived from qualitative inspection of the NOESY cross peaks. Thus, interproton distance constraints (a total of 60) were obtained by volume integration of the 200-ms NOESY and categorization of the intensities into the typical strong (1.8–2.7 Å)/medium (2.4–3.5 Å)/weak (3.2–4.6 Å) interactions (see Figure 8). Only stereospecifically assigned protons were used as constraining pairs. Dynamics simulations were performed solely as a monitor of the ability of the model helix to accommodate the experimental constraints.

Shown in Figure 9 are stereo overlays of structure snapshots taken at 32, 34, 36, 38, and 40 ps of the dynamics simulation. We note that while this is a qualitative treatment of the data, it is important that the structures obtained from the dynamics simulations do not exhibit significant deviations from the model helix geometry. Qualitatively similar structures are obtained if the restrained MD calculations start from a random conformation (R. Meadows, unpublished). Note also that the C-terminal segment, which was largely unconstrained, did not converge to a uniform topology.

The alternate conformation constraint set produced structures that were consistent with the major conformation structures in most respects. This result is not unexpected since there were only seven different constraints between the major and minor sets, and these differences were for residues 20–25. A comparison of residues 16–26 for the 38-ps minor and major conformation structure starting from the helical model is given in Figure 10. In the minor form, medium/longer range NOEs are observed between Gln*-20 α-H and Tyr*-22 NH, between Tyr*-22 α-H and Arg*-24 NH, and between Gln*-20 NH and Thr*-25 NH (Figure 8). These are not observed in the major conformer. As shown in Figure 10B, the minor form constraint set (see Results as well) allows Arg-24 and Thr-25 tight association with residues 20 and 21. The reminder of the C-terminal segment in the minor conformation simulation behaved as did the major conformer in that it did not converge on a consistent structure.

Conclusions

An α-helix for sCT bound to micelles and in methanol has been proposed on the basis of CD data and the regular spacing of hydrophobic and hydrophilic amino acids to begin as near to the loop as Val-8 and end at Pro-23. The NMR data derived from methanol/water system, show considerable α-helical character, in agreement with the CD data.

These results contrast those reported for sCT in 90% DMSO/10% H_2O (Motta et al., 1989) where evidence for an overall random coil structure with a short region of β-sheet and two tight turns was presented. Interestingly, an amide resonance positioned ~0.5 ppm downfield from the other amide protons is observed in both DMSO (Motta et al., 1989) and MeOH. In DMSO this resonance was assigned to Ser-13 while in methanol it is assigned to Leu-4 (see Figure 5). The Ser-13 NH peak in our methanoic sample was assigned to a resonance in the center of the amide/aromatic region perhaps indicative of the very great differences in the two structures.

It is clear from the NMR data in MeOH that at least two distinctly different conformations exist around the Pro-23 residue. The origin of the multiple conformations is believed to result from the cis–trans isomerism of Pro-23. The conformational variability can be seen to start at Gln-20 and can be assigned from Gln-20 through Thr-25. It has been shown, however, that two of the three "extra" threonine residues, identified from multiple NH to CH_3 cross peaks, there Thr-21 and Thr-25. It is interesting to ask whether the effectiveness of sCT as a therapeutic agent could be enhanced by "locking" the Pro-23 residue into a trans or cis conformation or whether such a modification would decrease efficacy because of lost flexibility upon interaction with its receptor.

Acknowledgments

We greatly appreciate the contributions of Dr. Vikram Roongta and the gift from Armour Pharmaceutical of the calcitonin.

References

Avramides, A., Baker, R. K., & Wallach, S. (1974) *Metabolism 23*, 1037–1046.

Azria, M. (1989) *The Calcitonins Physiology* and *Pharmacology*, S. Karger AG, Basal, Switzerland.

Braunschweiler, L, & Ernst, R. R. (1983) *J. Magn. Reson. 53*, 521–528.

Davis, D. G., & Bax, A. (1985) *J. Am. Chem. Soc. 107*, 2820–2821. Epand, R. M., Epand, R. F., Orlowski, R. C., Schlueter, R. J., Boni, L. T., & Hui, S. W. (1983) *J. Am. Chem. Soc 22*, 5074–5084.

Epand, R. M., Epand, R. F., & Orlowski, R. C. (1988) *Biochem. Biophys. Res. Commun. 152*, 203–207.

Ferrin, T. E., & Langridge, R. (1980) *Comput. Graphics 13*, 320.

Gobelet, C. (1986) *Schweiz. Rundsch. Med./Prax. 75*, 7–9.

Gorenstein, D. G., Meadows, R. P., Metz, J. T., Nikonwoicz, E., & Post, C. B. (1990) *Advances in Biophysical Chemistry* (Bush, C. A., Ed.) JAI Press, Greenwich, CT (in press).

Grob, K.-H. & Kalbitzer, H. R. (1988) *J. Magn. Reson. 76*, 87–99.

Hosking, D. J., & Heller, S. R. (1986) *Eur. J. Clin. Pharmacol. 31*, 27–31.

Inagaki, F., Shimada, I., Kawaguchi, K., Hirano, M., Terasawa, I., Ikura, T., & Gō, N. (1989) *Biochemistry 28*, 5985–5991.

Jeener, J., Meier, B. H., Bachmann, P. J., & Ernst, R. R. (1979) *J. Chem. Phys. 71*, 4546–4553.

Kallio, D. M., Garant, P. R., & Minkin, C. (1972) *J. Ultrastruct. Res. 39*, 205-216.
Kumar, A., Wagner, G., Ernst, R. R., & Wuthrich, K. (1981) *J. Am. Chem. Soc. 103*, 3654-3658.
Motta, A., Morelli, M. A., Goud, N., & Temussi, P. A. (1989) *Biochemistry 28*, 7996-8002.
Muller, N., Ernst, R. R., & Wuthrich, K. (1986) *J. Am. Chem. Soc. 108*, 6482-6492.
Niall, H. D., Keutmann, H. T., Copp, D. H., & Potts, J. T., Jr. (1969) *Proc. Natl. Acad. Sci. U.S.A. 64*, 771-778.
Orlowski, R. C., Safford, A. R., & Epand, R. M. (1987) *Eur. J. Biol. 162*, 399-402.
Piantini, U., Sorensen, O. W., & Ernst, R. R. (1982) *J. Am. Chem. Soc. 104*, 6800-6801.
Potts, J. T., Jr., Keutmann, H. T., Deftos, L. J., & Niall, H. D. (1972) *Proc. Pept. Res/Proc. Am. Pept. Symp.*, 93-105.
Wallach, S., Cohn, S. H., Atkins, H. L., Ellis, K. J., Kohberger, R., Aloia, J. F., & Zanzi, I. (1977) *Curr. Ther. Res. 22*, 556.
Weiner, P. K., & Kollman, P. A. (1981) *J. Comput. Chem. 2*, 287.
Wuthrich, K. (1986) *NMR of Proteins and Nucleic Acids*, John Wiley and Sons, New York.

Photoacoustic Calorimetric Study of the Conversion of Rhodopsin and Isorhodopsin to Lumirhodopsin†

Kathleen Marr and Kevin S. Peters*
Department of Chemistry and Biochemistry, University of Colorado, Boulder, Colorado 80309-0215
Received June 5, 1990; Revised Manuscript Received October 11, 1990

ABSTRACT: The enthalpy and volume changes for the conversion of rhodopsin and isorhodopsin to lumirhodopsin have been investigated by time-resolved photoacoustic calorimetry. The conversion of rhodopsin to lumirhodopsin is endothermic by 3.9 ± 5.9 kcal/mol and is accompanied by an increase in volume of 29.1 ± 0.8 mL/mol. The lumirhodopsins produced from rhodopsin and isorhodopsin are energetically equivalent.

The bleaching of the vertebrate photoreceptor rhodopsin initiates a series of enzymatic reactions leading to visual transduction (Fung et al., 1981). The first step in the enzymatic cascade is the association of a GTP-binding protein, transducin, with photoactivated rhodopsin (Baehr et al., 1982; Wessling-Resnick & Johnson, 1987). Rhodopsin is an integral membrane protein (39 kDa) located in disk membranes of the rod outer segment (ROS)[1] of the retina. This glycoprotein consists of an apoprotein, opsin, and a chromophore, 11-*cis*-retinal, attached via a protonated Schiff base. Following absorption of a photon, the chromophore undergoes an isomerization to the all-trans form, which causes the protein to thermally evolve through a series of conformational changes that are revealed as spectroscopically distinct metastable species (Birge, 1990). The dynamics of the decay of these metastable species have been well characterized at ambient temperatures (Applebury, 1984).

$$\underset{(498\ \text{nm})}{\text{rhodopsin}} + h\nu \xrightarrow{<6\ \text{ps}} \underset{(540\ \text{nm})}{\text{batho}} \xrightarrow{50\ \text{ns}} \underset{(497\ \text{nm})}{\text{lumi}} \xrightarrow{0.3\ \text{ms}} \underset{(478\ \text{nm})}{\text{metal}} \xrightarrow{10\ \text{ms}} \underset{(380\ \text{nm})}{\text{meta II}}$$

One of rhodopsin's intermediates, metarhodopsin II, is believed (Fung et al., 1981; Wessling-Resnick & Johnson, 1987) to be the active species that associates with transducin. The association of the two proteins effects an exchange of GTP for GDP on the α subunit of transducin. Subsequently, the α subunit of transducin binds to a phosphodiesterase, which leads to the hydrolysis of cGMP. The resulting decrease in cGMP concentration closes the Na^+ channels of ROS, causing a hyperpolarization of the plasma membrane (Fung et al., 1981).

The molecular basis by which photoactivated rhodopsin binds to transducin has not been formulated. Before a molecular model for the mechanism can be developed, the energetics of the reaction must be understood; thus a reaction energy profile for the bleaching of rhodopsin to form its various metastable species is required. In a very elegant series of photocalorimetry studies of the bleaching of rhodopsin, Cooper (1981) generated a reaction energy profile for the bleaching of rhodopsin and its evolution through the metarhodopsin II stage. The energetics of each intermediate were measured by trapping the metastable species at low temperatures where they were kinetically stable. For the first two intermediates, bathorhodopsin and lumirhodopsin, this entailed trapping in a low-temperature glycerol/water glass (Cooper, 1981; Schick et al., 1987).

In order for photolyzed rhodopsin to activate transducin, it is reasonable to speculate that the rhodopsin undergoes a series of structural changes within the portion of the protein that is exposed to the cytoplasm, which contains transducin (Kuhn et al., 1982). This may entail an increase or decrease in the volume of the protein. In addition, the change in conformation of the protein may lead to the exposure or the burying of charged groups. Thus, examining the energetics of rhodopsin's intermediates in a low-temperature glycerol/water glass may perturb the energetics of protein conformational changes as well as the energetics associated with the

† This research is supported by a grant from the National Institutes of Health (EY07510).

[1] Abbreviations: ROS, rod outer segment; HEPES, *N*-(2-hydroxyethyl)piperazine-*N'*-2-ethanesulfonic acid; CTAB, cetyltrimethylammonium bromide; BCP, bromocresol purple.

0006-2960/91/0430-1254$02.50/0